Development of Translucent Oxyapatite Ceramics by Spark Plasma Sintering

Yiqiang Shen,[‡] Jinling Xu,[§] Alfred Tok,[‡] Dingyuan Tang,[¶] Khiam Aik Khor,[§] and Zhili Dong[†,‡]

[‡]*School of Materials Science and Engineering, Nanyang Technological University, Singapore, Singapore*

[§]*School of Mechanical & Aerospace Engineering, Nanyang Technological University, Singapore, Singapore*

[¶]*School of Electrical & Electronic Engineering, Nanyang Technological University, Singapore, Singapore*

Author to whom correspondence should be addressed. e-mail: zldong@ntu.edu.sg

The pure $Sr_2Y_8(SiO_4)_6O_2$ oxyapatite powder materials have been ball milled and spark-plasma sintered. The microstructures and transmittances in the completely and incompletely densified ceramics were investigated. The ceramic sintered at 1500 ℃ is translucent with 0.7% porosity and its total forward light transmittance can reach about 52% in the infrared region. The transmittance was interpreted based on the microstructures of the ceramic samples and the Mie scattering theory.

I. Introduction

Silicate oxyapatites, a group of apatite materials, has a hexagonal crystal structure with a general formula $A^{I}_4A^{II}_6(SiO_4)_6O_2$, where A^{I} and A^{II} stand for two different Wycoff sites 4*f* and 6*h* that can be occupied by various cations.[1] Due to its good thermal and chemical stability and high crystal field,[2] silicate oxyapatites such as $Sr_2Y_8(SiO_4)_6O_2$ have been utilized in solid-state lasers and scintillators.[3–5] As both of the applications require bulk transparent materials, single crystals of silicate oxyapatites

were used in most of the previous studies. Because of the high melting point of the silicate oxyapatites,[6] Czochralski method is mostly used to grow the single crystals, though it is costly and time consuming. An alternative method to produce bulk transparent materials is to obtain sintered transparent polycrystalline ceramics, which is cost effective and fast in processing. In addition, transparent ceramics can be fabricated into larger sizes with improved mechanical properties.[7] In order to fabricate transparent ceramics, the light scattering centers inside the material, including pores, impurity phases, rough surfaces, and grain boundaries, must be minimized or eliminated.[8] The scattering effect of the pores is predominant because the porosity as low as 0.1% can deteriorate the transparency.[9]

So far, very few attempts to fabricate transparent silicate oxyapatite ceramics have been reported. In this work, the silicate oxyapatite $Sr_2Y_8(SiO_4)_6O_2$ was sintered by the spark plasma sintering (SPS) with the attempt to obtain condensed even transparent ceramics. The SPS is a promising way to produce densified ceramics[10–14] and it could heat the sample with a high heating rate due to the spark plasma generated by high-pulsed electric current.[15] The pure $Sr_2Y_8(SiO_4)_6O_2$ material were synthesized through solid-state reaction. After SPS translucent $Sr_2Y_8(SiO_4)_6O_2$ ceramics were obtained and the microstructures and transmittances in the completely and partially densified ceramics were investigated. Moreover, the in-line transmittance was analyzed by the Mie scattering theory.[16,17]

II. Experimental Procedure

The synthesis process of the pure $Sr_2Y_8(SiO_4)_6O_2$ powder was introduced elsewhere.[18] The resultant $Sr_2Y_8(SiO_4)_6O_2$ powders were further ball milled using zirconia balls and ethanol for 6 h. A SPS system (Sumitomo Coal Mining SPS system, Dr. Sinter Modal 1050, Tokyo, Japan) was used to prepare the consolidated ceramics. A 2 g sample was placed in a graphite die and aligned in the SPS chamber. The samples were first heated to 600 ℃ with a heating rate of 300 ℃/min and held for 1 min for stabilization. After that the temperature was increased to the sintering temperature

(1400 °and 1500 ℃) with a heating rate 100 ℃/min and dwelled 3 min. During the whole process, the pressure applied on the graphite die was kept at 23 MPa and the temperature profile was monitored by a pyrometer. The as-SPSed ceramic pellets were heat treated at 1400 ℃ for 1 h in a muffle furnace to remove the residual carbon on the surface as well as other defects. The surfaces of the two pellets were carefully polished by sand papers and diamond pastes to reduce the effect of rough surfaces. Both samples have a final thickness of 0.8 mm.

The phase compositions of the as-synthesized samples were studied using a Shimadzu 6000 X-Ray Diffractometer (XRD, Shimadzu, Kyoto, Japan) with a Cu-tube operated at 40 kV and 30 mA. The scan range of XRD is 10 °–80 °. The sizes of the powders and the surface morphologies of the ceramics were observed using a JEOL JSM-6340F scanning electron microscope (SEM, JEOL, Tokyo, Japan) with a field emission source. The grain sizes at the sample surface were measured from the SEM image and a correction factor 1.56 was used.[19] The total forward transmittance is the term including all the light passed through the sample in –180 °to 180 °range. It was measured by the Lambda 1050 UV/VIS/IR spectrometer equipped with the integration sphere (Perkin Elmer, Waltham, MA) in the range from 400 to 800 nm. For the in-line transmittance only the transmitted light in the same direction as the incident light is considered. It was measured by Cary 5000 UV-VIS-NIR spectrophotometer (Varian, CA) in the range from 200 to 810 nm. The densities of the ceramic pellets were measured using the Archimedes method.

The effective scattering coefficients of the birefringence and pores for the in-line transmittance and the angular dependence of the scattered light were calculated by the Mie scattering theory. All the calculations of Mie scattering used an algorithm written by Bohren and Huffman[17] coded in Fortran.

III. Results and Discussion

The XRD patterns of the as-synthesized $Sr_2Y_8(SiO_4)_6O_2$ powders and the ceramics SPSed at 1400 ° and 1500 ℃ are shown in Fig. 1. The consistency between calculated[18] and experimental patterns indicates that all samples

consisted of pure hexagonal oxyapatite phase. Therefore, the authors assumed that the light scattering effect from the impurity phase in the ceramic samples could be excluded.

The SEM image of the $Sr_2Y_8(SiO_4)_6O_2$ powders after horizontal ball milling is shown in Fig. 2. The powder is uniform and well dispersed. The average particle size measured from the SEM image is 0.77 μm.

The ceramics SPSed at 1400 °C and 1500 °C were chosen to investigate due to their shrinkage curves during the SPS (Fig. 3). The densification process was continuing until the temperature reached 1500 °C. Moreover, no further densification occurred during the dwell region in both 1400 °C and 1500 °C shrinkage curves. Therefore, the difference of the microstructures and transmittances in the completely and partially densified ceramics could be revealed by the comparison between the ceramics sintered at 1400 °C and 1500 °C. The density measurement shows that the relative densities of the ceramics SPSed at 1400 °C and 1500 °C are 98.1% and 99.3%, respectively. The porosity of the 1400 °C sintered sample (1.9%) is almost three times than that of the 1500 °C sintered one (0.7%). The pores observed by SEM (Fig. 4) are closed ones. The residual pores of the 1500 °C sintered sample are located at the junctions of the grains with a size of about 80 nm. Whereas the pores in the 1400 °C sintered sample are about 580 nm, which are larger (Fig. 4). All the results obtained from the density measurements and the SEM are consistent with the sintering shrinkage curve (Fig. 3). The curve shows that the densification process is not finished until 1450 °C so the densification did not complete for the sample sintered at 1400 °C, which results in higher porosity and larger pore size. The grain size range for both of the ceramics is about 0.5–9 μm. The average grain size of the ceramic SPSed at 1500 °C and 1400 °C is 3.8 and 3.2 μm, respectively. The grain growth of the ceramics is suppressed by the high heating rate of SPS. Frequently nanopowders are used in the SPS studies due to their good sinterability,[2,15,20] while the micrometer scaled powders used in this study are also suitable for SPS and detailed studies on the sintering behavior of the micrometer scale powders are undergoing.

The optical images of the ceramics SPSed at 1400 °C and 1500 °C are shown in Fig. 5. Both samples are translucent and the sample SPSed at 1400 °C apparently has

lower transparency due to the higher porosity and the larger pore size (Fig. 4). The sample SPSed at 1500 ℃ is translucent and the letters beneath can be displayed. The total forward transmittance and the in-line transmittance are almost zero for the opaque sample sintered at 1400 ℃. For the one sintered at 1500 ℃, both the total forward transmittance and the in-line transmittance increase as the wavelength increases (Fig. 6). The total forward transmittance reaches about 52% in the infrared region while the in-line transmittance is relatively low (3.2% at 800 nm). The large difference between the total forward transmittance and the in-line transmittance of the present sample indicates that large portion of the forward light was deflected by the grain boundaries and the residual pores, and that is why the letters beneath the ceramic become blur when the ceramic is lifted by several millimeters.

The in-line transmittance T for a sample with certain thickness can be expressed as

$$T = (1 - R)^2 \exp(-C_{\text{sca}} t) \tag{1}$$

where R is the reflectivity, C_{sca} is the effective scattering coefficient which should consider all the scattering centers, and t is the thickness of the sample. The reflectivity R can be derived from the refractive index of material n and the air $n' = 1$:

$$R = \frac{(n - n')^2}{(n + n')^2} \tag{2}$$

Because the refractive index of $Sr_2Y_8(SiO_4)_6O_2$ is unavailable, the data of $n_o = 1.831$ and $n_e = 1.816$ from a very similar compound $Ca_2Y_8(SiO_4)_6O_2$ were used.[6] The difference of the refractive index values of $Sr_2Y_8(SiO_4)_6O_2$ and $Ca_2Y_8(SiO_4)_6O_2$ is estimated to be about 3% by Lorenz–Lorentz formula. This difference is in an acceptable range and the approximation of the refractive index is feasible. Therefore, the calculations followed can reflect the light transmittance characteristics in $Sr_2Y_8(SiO_4)_6O_2$. The calculated R value is about 0.84. As $Sr_2Y_8(SiO_4)_6O_2$ is

optically anisotropic due to the hexagonal crystal structure, the C_{sca} should include both the scattering caused by the pores and the birefringence effect:

$$C_{sca} = C_{pore} + C_{bi} \tag{3}$$

The effective scattering coefficient of pore C_{pore} can be expressed by the terms of porosity and pore radius[21]:

$$C_{pore} = N_{pore} G_{pore} Q_{pore} = \frac{3V_p}{4r_{pore}} Q_{pore} \tag{4}$$

Where N_{pore} is the pore density, G_{pore} is the geometrical cross section of pore, r_{pore} is the radius of the pores, V_p is the volume % of porosity, and Q_{pore} is the scattering efficiency of pore.

The effective scattering coefficient of the birefringence can be calculated based on the model proposed by Apetz and Bruggen[9]:

$$C_{bi} = N_{bi} G_{bi} Q_{bi} = \frac{1}{2} \frac{1}{\frac{4}{3}\pi r_{bi}^3} Q_{bi} \tag{5}$$

Where N_{bi} is the number of the scattering centers causing birefringence effect, G_{bi} is the geometrical cross section, r_{bi} is the radius of the scattering centers, and Q_{bi} is the scattering efficiency. In order to calculate the scattering efficiencies Q_{bi} and Q_{pore} and the effective scattering coefficients C_{bi} and C_{pore} for the two ceramics sintered at 1400 °and 1500 ℃, the results from the SEM images and the density measurements are used (V_p (1500 ℃) = 0.7%, V_p (1400 ℃) = 1.9%, r_{bi} (1500 ℃) = 1.9 μm, r_{bi} (1400 ℃) = 1.6 μm, r_{pore} (1500 ℃) = 40 nm, and r_{pore}(1400 ℃) = 580 nm). The calculated results for both ceramics sintered at 1400 ° and 1500 ℃ are shown in Fig. 7. Due to their similar grain sizes for the 1400 ° and 1500 ℃ sintered ceramics, the difference of their C_{bi} derived from Eq. (5) are small, demonstrating their similar influence on the light scattering. The C_{pore} for both 1400 ° and 1500 ℃ sintered ceramics are

higher than their C_{bi} values, exhibiting more pronounced scattering influence on the in-line transmittance. Due to the higher porosity and larger pore size, the value of C_{pore} for the sample sintered at 1400 ℃ is much larger; therefore the light transmittance of the material is poor.

Using the effective scattering coefficients obtained above, the in-line transmittance of the 1500 ℃ sintered sample was calculated from Eq. (1). The difference of the experimental and calculated transmittance values is small at longer wavelength, whereas the experimental values are much higher than the calculated ones at shorter wavelength. This phenomenon is also exhibited in Yamashita *et al*.[22]. The difference may be ascribed to the fact that only the average pore size is used in the above discussion. It is believed that the pore size distribution can cause difference between the calculated and experimental curves as indicated in Fig. 6. For more accurate calculations, the pore size distribution needs to be considered, which will be investigated in our future research.

IV. Conclusion

In summary, the translucent silicate oxyapatite $Sr_2Y_8(SiO_4)_6O_2$ ceramic with hexagonal crystal structure was successfully fabricated by using the SPS in combination with the conventional solid-state reaction. The microstructures and transmittances in the completely and partially densified ceramics sintered by SPS were investigated. The porosity of the ceramic sintered at 1500 ℃ is about 0.7%, the total forward light transmittance has reached 52% in the infrared region. The total forward transmittance is mainly influenced by the residual pores, while the in-line transmittance is affected by both birefringence effect and residual pores. As the residual pores affect the light transmittance much more severely than the birefringence effect according to the effective scattering coefficients, it is important to eliminate residual pores in the fabrication of transparent ceramics.

References

[1] J. Felsche, "Crystal Chemistry of Rare-Earth Silicates," *Acta Crystallogr., Sect. A: Found.*, **28**, 108 (1972).

[2] A. Yoshikawa, C. Fujiwara, H. Sato, T. Nishi, H. Ohta, T. Fukuda, Y. Waseda, G. Boulon, M. Ito, Y. Guyot, and K. Lebbou, "Czochralski Growth of Yb Doped Oxyapatites for High Power Laser Application," *Opt. Mater.*, **26**, 385–90 (2004).

[3] B. Francois, M. Navizet, J. Rebreyend, and C. Won, "Monocrystals of Silicates of Lanthanides Usable as Scintillators for the Detection of X and Gamma Radiation"; U.S. Patent No. 4988882, 1991.

[4] F. Druon, S. Chenais, and F. Raybaut, "Apatite-Structure Crystal, Yb^{3+}: $SrY_4(SiO_4)_3O$, for the Development of Diode-Pumped Femtosecond Lasers," *Opt. Lett.*, **27** [21] 1914–6 (2002).

[5] F. Druon, F. Balembois, and P. Georges, "Ultra-Short-Pulsed and Highly-Efficient Diode Pumped Yb:SYS Mode-Locked Oscillators," *Opt. Express*, **12** [20] 5005–12 (2004).

[6] K. B. Steinbruegge, T. Henningsen, R. H. Hopkins, R. Mazelsky, N. T. Melamed, E. P. Riedel, and G. W. Roland, "Laser Properties of Nd^{+3} and Ho^{+3} Doped Crystals with Apatite Structure," *Appl. Opt.*, **11** [5] 999–1012 (1972).

[7] V. Lupei, A. Lupei, N. Pavel, T. Taira, Y. Sato, and A. Ikesue, "Comparison of Nd : YAG Single Crystals and Transparent Ceramics as Laser Materials," *Proc. SPIE*, **5581**, 212–9 (2004).

[8] K. Hayashi, O. Kobayashi, S. Toyoda, and K. Morinaga, "Transmission Optical-Properties of Polycrystalline Alumina with Submicron Grains," *Mater. Trans. JIM*, **32** [11] 1024–9 (1991).

[9] R. Apetz and M. P. B. Bruggen, "Transparent Alumina: A Light-Scattering Model," *J. Am. Ceram. Soc.*, **86** [3] 480–6 (2003).

[10] R. Chaim, R. Marder-Jaeckel, and J. Z. Shen, "Transparent YAG Ceramics by Surface Softening of Nanoparticles in Spark Plasma Sintering," *Mater. Sci. Eng. A*, **429** [1–2] 74–8 (2006).

[11] M. Suarez, A. Fernandez, J. L. Menendez, and R. Torrecillas, "Grain Growth Control and Transparency in Spark Plasma Sintered Self-Doped Alumina Materials," *Scr. Mater.*, **61** [10] 931–4 (2009).

[12] Z. J. Shen, M. Johnsson, Z. Zhao, and M. Nygren, "Spark Plasma Sintering of Alumina," *J. Am. Ceram. Soc.*, **85** [8] 1921–7 (2002).

[13] C. Wang and Z. Zhao, "Transparent $MgAl_2O_4$ Ceramic Produced by Spark Plasma Sintering," *Scr. Mater.*, **61** [2] 193–6 (2009).

[14] K. Morita, B. N. Kim, K. Hiraga, and H. Yoshida, "Fabrication of Transparent $MgAl_2O_4$ Spinel Polycrystal by Spark Plasma Sintering Processing," *Scr. Mater.*, **58** [12] 1114–7 (2008).

[15] M. Omori, "Sintering, Consolidation, Reaction and Crystal Growth by the Spark Plasma System (SPS)," *Mater. Sci. Eng. A*, **287** [2] 183–8 (2000).

[16] H. C. Van de Hulst, *Light Scattering by Small Particles*. Wiley, New York, 1957.

[17] C. F. Bohren and D. R. Huffman, *Absorption and Scattering of Light by Small Particles*. Wiley, New York, 1983.

[18] Y. Q. Shen, A. Tok, D. Y. Tang, and Z. L. Dong, "Synthesis and Crystal Structure Characterization of Silicate Apatite $Sr_2Y_8(SiO_4)_6O_2$," *J. Am. Ceram. Soc.*, **93** [4] 1176–82 (2010).

[19] M. I. Mendelson, "Average Grain Size in Polycrystalline Ceramics," *J. Am. Ceram. Soc.*, **52** [8] 443–6 (1969).

[20] R. Chaim, Z. J. Shen, and M. Nygren, "Transparent Nanocrystalline MgO by Rapid and Low-Temperature Spark Plasma Sintering," *J. Mater. Res.*, **19** [9] 2527–31 (2004).

[21] J. Peelen and R. Mestselaar, "Light Scattering by Pores in Polycrystalline Materials: Transmission Properties of Alumina," *J. Appl. Phys.*, **45** [1] 216–20 (1973).

[22] I. Yamashita, H. Nagayama, and K. Tsukuma, "Transmission Properties of Translucent Polycrystalline Alumina," *J. Am. Ceram. Soc.*, **91** [8] 2611–6 (2008).

List of Figures

(down-triangle) in the ceramic sintered at 1500 ℃.

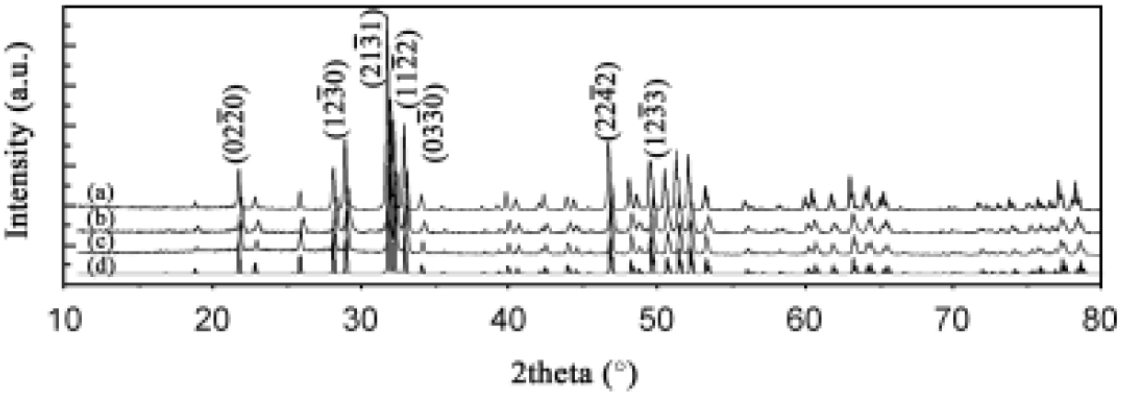
Intensity (a.u.)
(02$\bar{2}$0)
(12$\bar{3}$0)
(21$\bar{3}$1)
(11$\bar{2}$2)
(03$\bar{3}$0)
(22$\bar{4}$2)
(12$\bar{3}$3)
(a)
(b)
(c)
(d)
10
20
30
40
50
60
70
80
2theta (°)

Fig. 1.

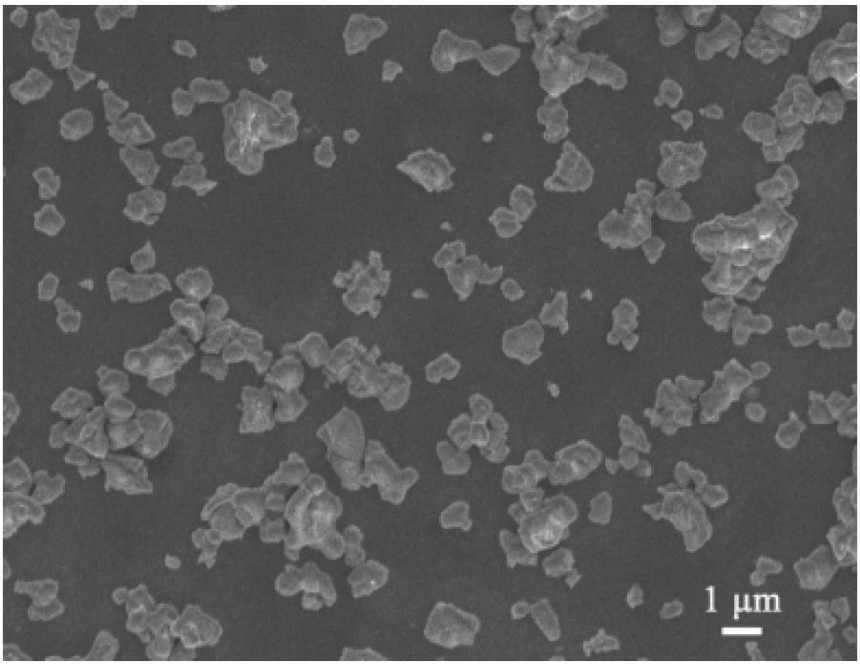

Fig. 2.

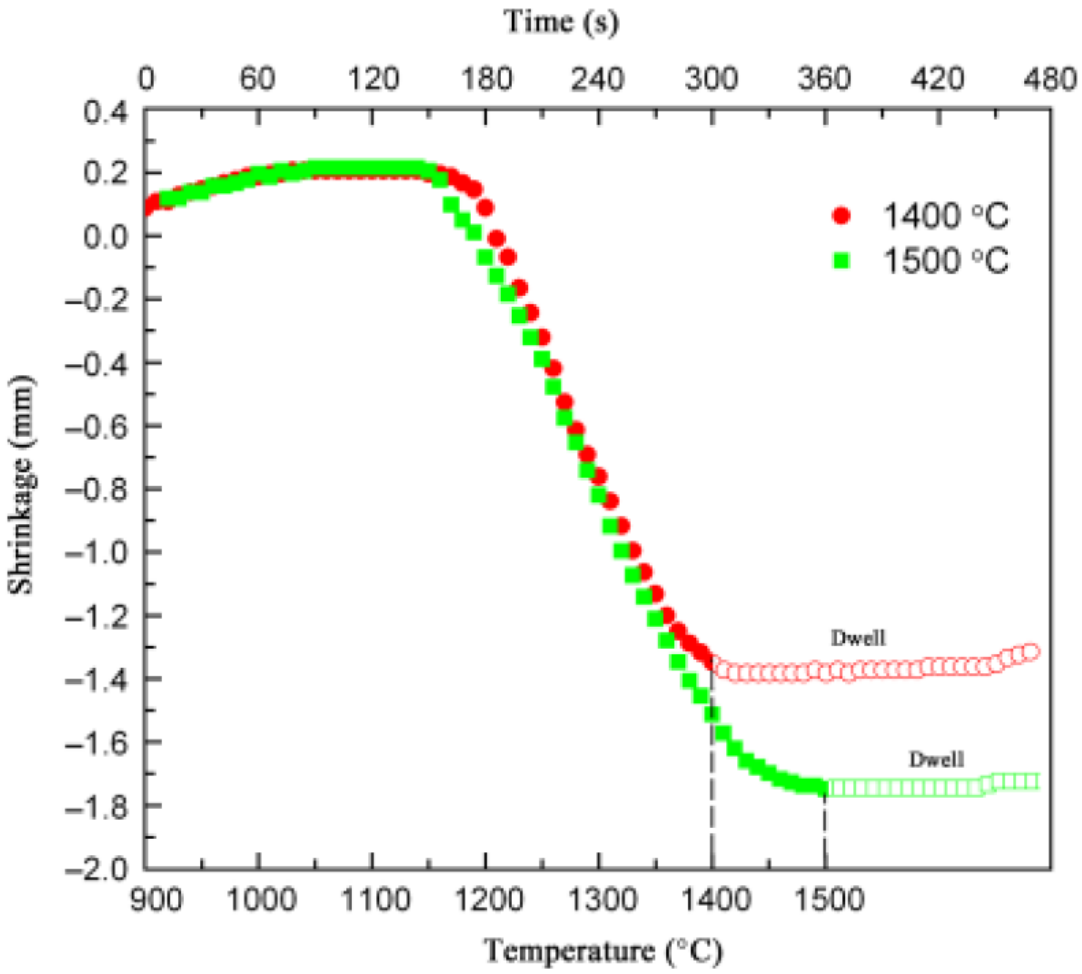
Time (s)
0
60
120
180
240
300
360
420
480
0.4
0.2
0.0
−0.2
−0.4
−0.6
−0.8
−1.0
−1.2
−1.4
−1.6
−1.8
−2.0
Shrinkage (mm)
1400 °C
1500 °C
Dwell
Dwell
900
1000
1100
1200
1300
1400
1500
Temperature (°C)

Fig. 3.

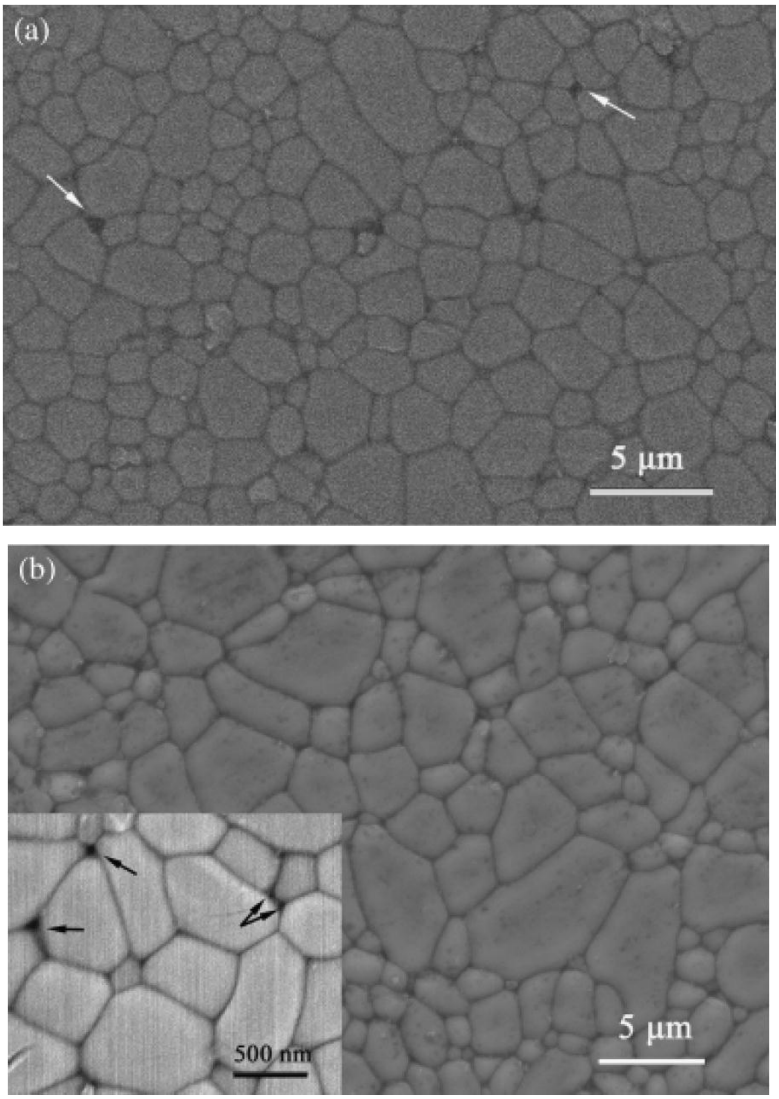

Fig. 4.

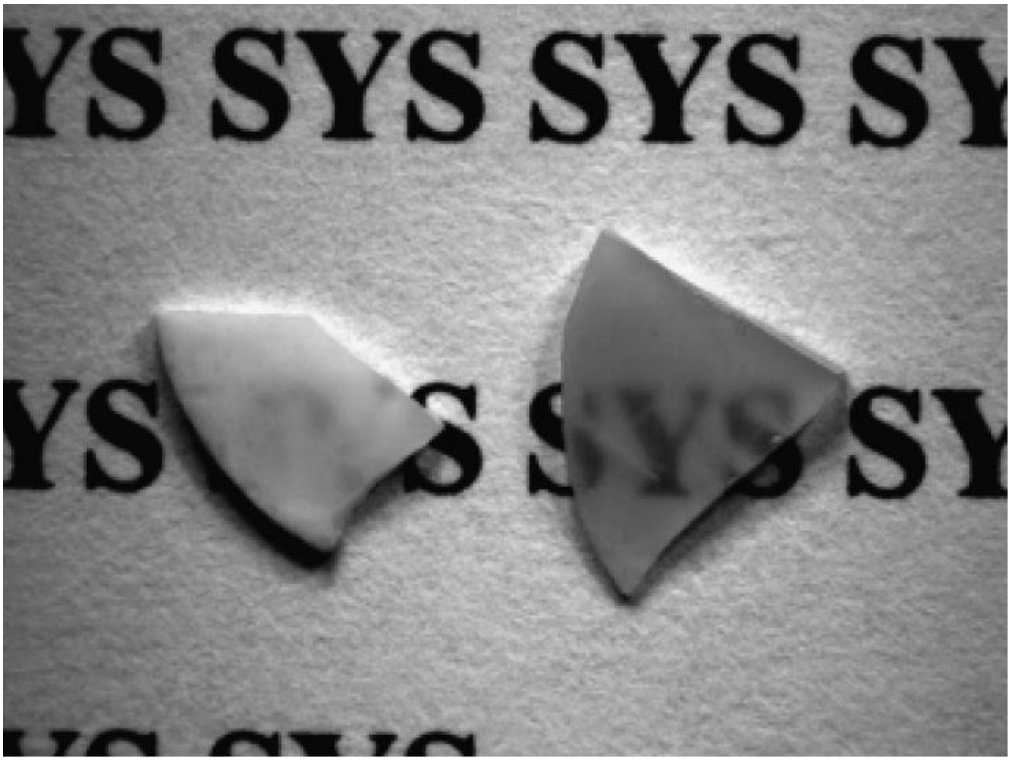

Fig. 5.

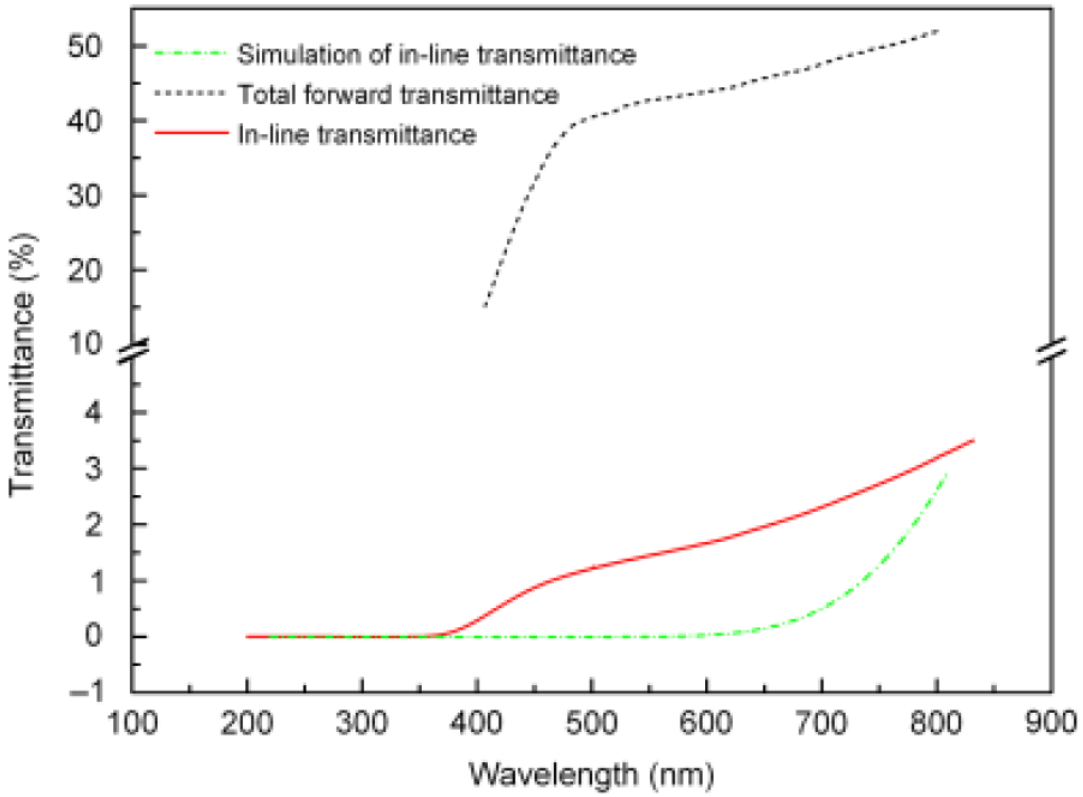
Simulation of in-line transmittance
Total forward transmittance
In-line transmittance
Transmittance (%)
Wavelength (nm)
50
40
30
20
10
4
3
2
1
0
−1
100
200
300
400
500
600
700
800
900

Fig. 6.

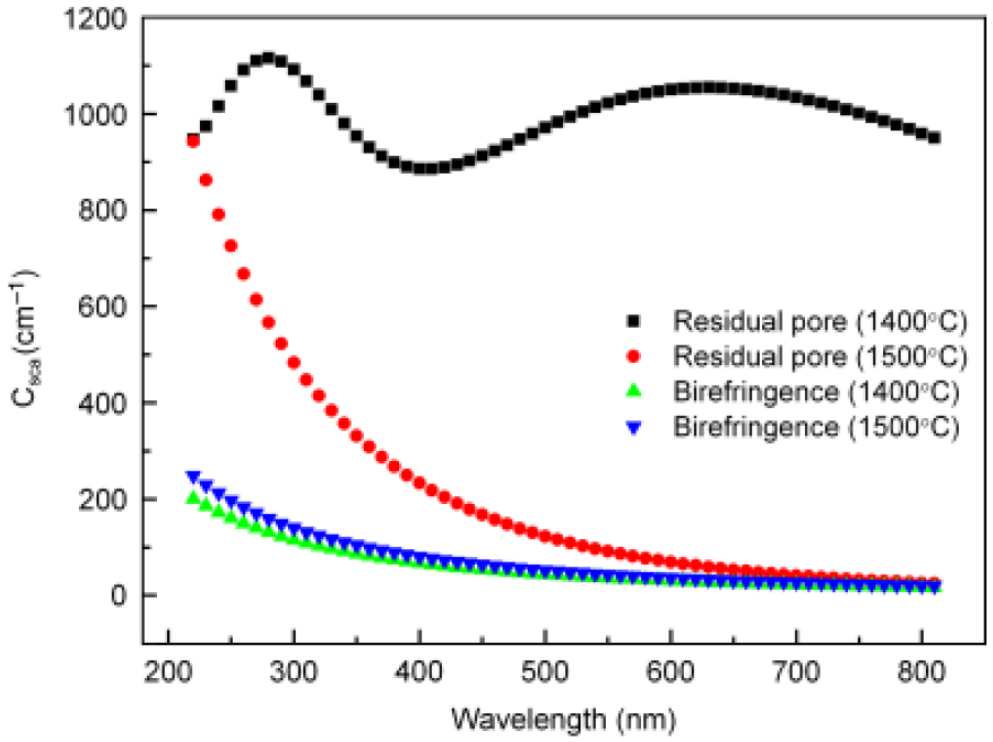
1200
1000
800
600
400
200
0
C_{sca} (cm^{-1})
200
300
400
500
600
700
800
Wavelength (nm)
Residual pore (1400°C)
Residual pore (1500°C)
Birefringence (1400°C)
Birefringence (1500°C)

Fig. 7.